Geophys. J. R. astr. Soc. (1979) **59**, 497–522

Earthquake sequences on a frictional fault model with non-uniform strengths and relaxation times

Takeshi Mikumo and Takashi Miyatake *Disaster Prevention Research Institute, Kyoto University, Uji, Kyoto 611, Japan*

Received 1979 April 23; in original form 1979 January 2

Summary. The space and time characteristics of earthquake sequences, including a main shock, aftershocks and the recurrence of major shocks in a long time range, are investigated on a frictional fault model with non-uniform strengths and relaxation times, which is subjected to a time-dependent shear stress. Aftershocks with low stress drop take place successively in spaced regions so as to fill the gaps which have not yet been ruptured since the main shock, while those with high stress drop occur in and around the regions left unruptured during the main faulting. The frequency decay of aftershocks with time follows a hyperbolic law with the rates p consistent with observations. There are good linear relations in logarithmic scales for source area versus frequency and seismic moment versus frequency of the generated aftershocks. The b-value obtained in the present experiments appears slightly larger than that for observations. It was found that more heterogeneous distribution of the fault strength give smaller p and larger b-values. The recurrence of major shocks, particularly of very large shocks with high stress drop, is often preceded by a completely silent period of activity or very low activity with a small number of foreshocks. The major shocks take place successively in adjacent unruptured regions and sometimes show slow-speed migrations. These results provide explanations to various observations of earthquake sequences.

1 Introduction

It is widely accepted that earthquakes are the result of sudden shear faulting under increasing tectonic stress. Elastic dislocation models as well as crack models have so far been successfully applied to account for some of the general features of the faulting process. It now appears, however, that more realistic physical models are required to incorporate several important features of seismic faulting, which are often observed in the field and sometimes suggested also by laboratory experiments. These are: (1) initiation, spreading and stopping mechanism of rupture, (2) stick-slip instability of faulting, (3) radiation of high frequency seismic waves in the near-field, (4) non-uniform distribution of fault displacements, (5) occurrence of earthquake sequences – foreshocks, main shock sometimes

Downloaded from http://gji.oxfordjournals.org/ at Library of Research Reactor Institute, Kyoto University on December 7, 2014

followed by multiple shocks, and aftershocks – on the same fault, (6) frequency decay law of aftershocks, (7) magnitude–frequency relation for all shocks on the fault, (8) aseismic slip including pre-seismic and post-seismic fault movements, and so forth (e.g. Nur 1978).

We have investigated, in a previous paper (Mikumo & Miyatake 1978), the dynamical rupture process on a three-dimensional frictional fault, and have been able to provide satisfactory explanations to some of the above features by introducing, in a stochastic way, non-uniform distributions of static frictional strength with a finite shear stress into the fault. These non-uniformities may arise from heterogeneous structure and properties of fault gouge, irregular shape, local bending, the degree of contact of asperities on the fault surface, inhomogeneous pore pressures around there and so forth. Inhomogeneous shear stress distribution should also be taken into consideration in fault dynamics, but this results mainly from past fault slips. It is reasonable, therefore, to consider non-uniform strength as a basic property of the fault, although its details are not known directly from observations and surveys. Several investigators have also noticed the importance of heterogeneity and attempted to take it into their models (e.g. Dieterich 1972a; Knopoff, Mouton & Burridge 1973; Das & Aki 1977; Nur 1978; Israel & Nur 1979).

In the present paper, we will focus our attention particularly to the occurrence of earthquake sequences on the frictional fault. It has been shown (Mikumo & Miyatake 1978) that the final fault displacements and residual stresses after the main rupture have large variations if the frictional strength is heavily non-uniform, and that in some extreme cases there remain unruptured regions around which high stresses are concentrated. It has been also pointed out that these post-seismic situations could generate succeeding earthquakes under some conditions.

The mechanisms of aftershock occurrence proposed so far include: time-dependent creep recovery of rocks (Benioff 1951), transient stress recovery combined with time-dependent friction (Dieterich 1972a, b, 1978), the decrease in the shear strength of rocks due to pore fluid flow (Nur & Booker 1972) together with consolidation reloading (Booker 1974), time-delayed fractures of heterogeneous medium due to the weakening of the strength under concentrated stress (e.g. Mogi 1962b; Scholz 1968; Knopoff 1972) and stress corrosion cracking (Anderson & Grew 1977). Numerical simulations of aftershocks on one-dimensional models have been made with a viscous process (Dieterich 1972b; Cohen 1977) or with stress-induced crack nucleation (Rundle & Jackson 1977), but these one-dimensional models appear still incomplete to provide reasonable explanations to the actual mechanism of aftershocks.

Here, we investigate numerically the entire process of earthquake sequences including a main faulting, aftershocks and the recurrence of major shocks sometimes with foreshocks in a long time range, by introducing time-dependent shear stress and strength into the three-dimensional fault described in the previous paper (Mikumo & Miyatake 1978). The main purpose here is: (1) to investigate what types of shocks are generated with different stress drops, fault displacements and source areas, (2) to see if these simulated shocks could explain some empirical laws usually experienced in actual observations, and (3) to look for explanations to seismic gap in time and space prior to the occurrence of large earthquakes.

2 Fault model

The model we use here is essentially the same quasi-three-dimensional fault as treated in our previous paper (Mikumo & Miyatake 1978), henceforth referred to as Paper I, which is subjected to an external shear stress. With the aid of a three-dimensional mechanical model equivalent to the present problem, we have obtained dynamical solutions for rupture

Downloaded from http://gji.oxfordjournals.org/ at Library of Research Reactor Institute, Kyoto University on December 7, 2014

propagation and time history of stresses and slip displacements at discretized elements on the fault, taking into account the distribution of static and dynamic frictional stresses. After the main rupture over the fault, the initial shear stress drops nearly to the level of the dynamical frictional stress in the case of homogeneous or weakly non-uniform frictional strength, while the residual stress indicates large variations in the case of heavily non-uniform distribution of the strength. The frictional strength will also drop after the rupture in the slipped segments of the fault due to the decrease in static frictions (Dieterich 1972a) or due to the increase in pore fluid pressures (Nur & Booker 1972; Booker 1974).

Now we consider time-dependent recovery process of the shear stress and strength on the fault after the main faulting, in order to see how aftershocks and eventual shocks are generated under various conditions. Although there could be several possible mechanisms for the stress recovery, we think that a viscoelastic process represents a transient stress recovery due to creep of rocks (Dieterich 1972b) as well as of fault gouge material or due to consolidation of porous medium (Booker 1974).

We have considered several types of viscoelastic solids to approximate viscoelastic behaviour of fault gouge, but the one adopted here is a standard three-parameter linear solid, which includes a Maxwell element in parallel with an elastic spring. For this simple model, we have the following relation,

$$\sigma + \tau\dot{\sigma} = k(\alpha\epsilon + \tau\dot{\epsilon}) \tag{1}$$

where σ and ϵ represent the stress and strain, k is the unrelaxed elastic modulus, τ is the relaxation time under a constant strain and α implies a coefficient of the relaxed elastic modulus (e.g. Liu, Anderson & Kanamori 1976). For a complete, three-dimensional viscoelastic solid, the corresponding stress–strain relation may generally be written as,

$$\sigma_{kl} + \tau\dot{\sigma}_{kl} = \alpha(\lambda\Theta\delta_{kl} + 2\mu e_{kl}) + \tau(\lambda\dot{\Theta}\delta_{kl} + 2\mu\dot{e}_{kl}) \quad (k = 1, 2, 3;\ l = 1, 2, 3) \tag{2}$$

where λ and μ are Lamé's constants, Θ is the dilatation, and δ_{kl} is the Kronecker's delta.

As described in the previous paper, however, the model we consider here has a quasi-three-dimensional plate-like structure with a thickness of Δz bounded above by a rigid boundary and at the base by the fault plane. In this model, we deal with five stress–strain components ($k = 1, 2$; $l = 1, 2, 3$) on the fault ($z = 0$), assuming that $\sigma_{zz} = 0$ and $w = 0$ as $z \to 0$. The purpose here is to see viscoelastic stress change on the fault after the main faulting in response to elastic strain change due to the faulting, on the condition that all fault elements stick to their displaced position being resisted by static frictions after the dynamic motion was completed. This condition implies that there is no creep displacement thereafter. For this purpose, we simply treat the stress–strain relation for each of small fault elements, as a quasi-static problem without going into the equation of motion. Equation (2) for this case may then be simply transformed into the following form, by differentiating it with respect to x_l and summing them up,

$$\frac{\partial \tilde{F}_k}{\partial t} + \frac{\tilde{F}_k}{\tau} = \frac{\partial F_k}{\partial t} + \frac{\alpha F_k}{\tau} \tag{3}$$

where

$$\tilde{F}_k = \sum_{l=1}^{3} \frac{\partial \sigma_{kl}}{\partial x_l}, \quad F_k = \lambda \sum_{l=1}^{2} \frac{\partial e_{ll}}{\partial x_l} + 2\mu \sum_{l=1}^{3} \frac{\partial e_{kl}}{\partial x_l} \quad (k = 1, 2). \tag{4}$$

F_k may also be rewritten in the form of the right-hand side of equation (1) in Paper I, and approximated by equations (2) and (4) there for discretized grid points. This means that if

Downloaded from http://gji.oxfordjournals.org/ at Library of Research Reactor Institute, Kyoto University on December 7, 2014

we suppose such a three-dimensional mechanical model with mass and spring as schematically depicted in Paper I, $F_k(k = 1, 2)$ correspond to the x- and y-components of the elastic force per unit volume applied to a mass element located at (x_i, y_j) on the fault plane. F_k changes during dynamic faulting due to slip motion of the concerned and adjacent fault elements, and this change may be regarded as a sudden force drop at $t = T$ in a longer time interval. $\tilde{F}_k(k = 1, 2)$ indicate the corresponding viscoelastic force working on the element, which is resisted by the static frictional force after the faulting, in response to the input dynamic force change.

The external shear stress is also no longer constant over a long time range, but assumed to increase linearly due to the increase in tectonic loading such as the drag force of plate movement. Taking into account this stress increase, the elastic force change after $t = T$ may be expressed by two parts,

$$F_{1k}(t) = F_k(0) + C_k t, \quad F_{2k}(t) = -\Delta F_k \cdot H(t - T) \quad (k = 1, 2) \tag{5}$$

where $F_k(0)$ indicates an unknown elastic force at $t = 0$, and ΔF_k is the force change at $t = T$. C_k, the increasing rate of the tectonic force, may be written as $C_k = \mu \dot{U}_k/(\Delta z)^2$ in the present model, since the applied stress components σ_{zx} and σ_{yz} in equation (3) in Paper I may be replaced by $\sigma_{zx} \cong \mu(U_0 + \dot{U}t - u_{ij})/\Delta z$ and $\sigma_{yz} \cong \mu(V_0 + \dot{V}t - v_{ij})/\Delta z$. $t = 0$, T_- and T_+ are taken some time long before, just before and right after the main faulting. The viscoelastic response $\tilde{F}_k$ can be obtained by substituting each of the two parts in equation (5) into equation (3),

$$\begin{aligned}
&\tilde{F}_{1k}(t) \cong (1 - \alpha)C_k \tau + \alpha F_k(0) + \alpha C_k t = \tilde{F}_k(T_-) + \alpha C_k(t - T) \\
&\tilde{F}_{2k}(t) = -\alpha \Delta F_k - (1 - \alpha)\Delta F_k \cdot \exp\,[-(t - T)/\tau] \\
&\tilde{F}_k(t) = \tilde{F}_{1k}(t) + \tilde{F}_{2k}(t) \\
&\qquad = \tilde{F}_k(T_-) - \Delta F_k[\alpha + (1 - \alpha) \cdot \exp\,\{-(t - T)/\tau\}] + \alpha C_k(t - T) \quad (k = 1, 2).
\end{aligned} \tag{6}$$

The force change ΔF_k is taken positive here for the force drop due directly to the slip of the concerned fault element itself, and taken negative for the force rise resulting from the slip of adjacent elements. Equation (6) then indicates that for the slipped elements the dropped force will recover with time, whereas the concentrated high stress in the unruptured elements will be relaxed. If the force drops take place successively by N times in a form

$$-\sum_{n=1}^{N} \Delta F_{k,n} \cdot H(t - T_n)$$

due to aftershocks at $t = T_n(n = 1, 2, \ldots, N)$ within a time short compared with the relaxation time τ, the corresponding viscoelastic response may be expressed by,

$$\begin{aligned}
\tilde{F}_k(t) = \tilde{F}_k(T_{1-}) &- \sum_{n=1}^{N} \Delta F_{k,n}[\alpha + (1 - \alpha) \exp\,\{-(t - T_n)/\tau\}] \\
&- \sum_{n=2}^{N} (1 - \alpha)\Delta F_{k,n-1}[1 - \exp\,\{(T_n - T_{n-1})/\tau\}] + \alpha C_k(t - T_1) \quad (k = 1, 2).
\end{aligned} \tag{7}$$

Preliminary calculations show that the effects of the force drops at least three times before the rupture now in consideration should be taken into account (Miyatake 1978).

On the other hand, the frictional strength that dropped in the slipped elements of the fault after the main faulting slowly recovers with time (Dieterich 1972a; Scholz, Molnar & Johnson 1972; Engelder, Logan & Handin 1975) probably due to creep at points of contact

Downloaded from http://gji.oxfordjournals.org/ at Library of Research Reactor Institute, Kyoto University on December 7, 2014

on the fault surface (Dieterich 1978). If this time-dependent process follows the experimental formula by Dieterich (1978), $\mu_s(t) = \mu_s^0 + A \log(Bt + 1)$, the frictional strength $\sigma_s(t)$ after a shock at $t = T_n$ may be written as,

$$\sigma_s(t) = \sigma_s^0 + \delta\sigma_s \cdot \log [B(t - T_n) + 1] \tag{8}$$

where $\sigma_s(t) = \mu_s(t)\sigma_n$, $\sigma_s^0 = \mu_s^0\sigma_n$ and $\delta\sigma_s = A\sigma_n$ for a normal stress σ_n. $\mu_s(t)$ and μ_s^0 are the coefficients of static frictions at a time t and right after the rupture. A and B are numerical constants, and σ_s^0 and $\delta\sigma_s$ may be interpreted as the strength right after the rupture and its recovery rate, respectively. We assume that σ_s^0 may also be written as $\sigma_s^0 = C_d \cdot \sigma_s(T_{1-})$ by introducing a constant drop rate C_d with respect to the strength before the main faulting at $t = T_1$. However, if, instead, the weakening of the strength results from the increase in pore pressures due to fluid inflow around the fault (Nur & Booker 1972; Booker 1974), it will decrease slowly with time.

Now we assume that when the viscoelastically recovering shear stress exceeds the above time-dependent strength at a point on the fault, local slip will immediately take place on the concerned element. The fracture criterion we use here is, $\tilde{F} = (\tilde{F}x^2 + \tilde{F}y^2)^{1/2} \geqq Fs = \sigma_s(t)/\Delta z$, analogous to that in Paper I, where $\tilde{F}$ is the resultant viscoelastic force and Fs represents the static frictional force. Once this condition is satisfied, slip motion begins but is resisted by the dynamic frictional force. After this moment the rupture initiating from that point propagates on the fault and is developed into an aftershock with a size specified by the distribution of the shear stress and strength at that time. This is the dynamic rupture process which can be calculated as in the previous paper (Mikumo & Miyatake 1978).

3 Model parameters in numerical calculations

The main physical parameters that control the generation process of aftershocks and subsequent earthquake sequences are; static and dynamic frictional strengths σ_s and σ_d, the weakening and recovery rates of the static strength C_d and $\delta\sigma_s$, the relaxation time τ, the coefficient of the relaxed elastic modulus α, and the increasing rate of the tectonic force C_k. The last parameter has a large effect on the recurrence of future earthquakes but not on the generation of aftershocks. This will be discussed separately in a later section. Some of these parameters may be non-uniformly distributed on the fault because of heterogeneous properties of fault gouge, and hence will be varied from place to place in the present model. Besides these, elastic constants λ and μ, and Poisson's ratio may vary depending on the location. Although there might be some physical relationship between these parameters, we deal with them as independent in our numerical calculations.

Static frictional strength σ_s is distributed normal-randomly with a minimum of 200 bar and standard deviations of 10–30 bar, and also with extremely high strength inclusions reaching 500–700 bar. This type of distribution is simply assumed on the basis of the Weibull's distribution which can be found in some experimental studies on rock materials. Other types of distribution like Poisson's may be possible, to account for the observed magnitude–frequency relation for actual earthquakes (Nur 1978). Dynamic frictional strength σ_d is assumed to be constant, 100 bar in most of our calculations, but varied between 100 and 120 bar in proportion to the static strength in some other cases.

There could be several relaxation mechanisms for natural rocks existing in earth materials, and hence it may be more reasonable to consider the relaxation times τ distributed over a broad band rather than represented by a single value. Some estimates for the distribution range between 10–10^4 s (Liu *et al.* 1976), 2×10^{-2}–2×10^2 s (Savage 1965), 10^2–10^4 s (Lomnitz 1956; Dieterich 1972b) and 4×10^6 s (Itô & Sasajima 1979). If, instead, we con-

Downloaded from http://gji.oxfordjournals.org/ at Library of Research Reactor Institute, Kyoto University on December 7, 2014

sider consolidation reloading or dilatancy hardening of porous material due to fluid inflow around the fault as a possible mechanism for viscoelastic process (Booker 1974), the relaxation time would correspond to the time required for fluid diffusion, say 1–10 days. For these reasons, we assume several different cases; one is a constant relaxation time between 1.8×10^3 s (30 min) and 1.72×10^5 s (2 days), and the other in uniform-randomly distributed times between $1–10^3$ s, $9 \times 10^2–8.64 \times 10^4$ s (15 min–1 day), $6 \times 10^2–4.32 \times 10^5$ s (10 min–5 days) and so on.

The coefficient of the relaxed elastic modulus α specifies the upper bound of the recovered stress, as may be easily understood from equation (6). On the other hand, if the stress recovery is actually due to consolidation reloading, this process yields a stress rise of $\beta|\Delta\sigma|$ (Booker 1974), where $\beta = (1 - 2\nu)/2(1 - \nu)$ with Poisson's ratio ν. Comparing the final stress in these two cases, $\alpha = 1 - \beta$, although the recovery rates are somewhat different. For rock material, most probable values for α range between $0.62 < \alpha < 0.71$ for $0.2 < \nu < 0.3$ (or $1.63 < Vp/Vs < 1.89$). From this evidence, we assume several cases with a constant α between 0.60 and 0.74, and also with uniform-randomly distributed values in this range.

The weakening and recovery rates of the frictional strength may be estimated from experimental evidence by Dieterich (1972a, 1978). His results show that the coefficient of static friction μ_s increases by about 6–10 per cent during the time of stationary contact up to 10^5 s, and that μ_s^0, A and B take values between 0.6–0.8, 0.01–0.03 and 1.0–2.0, respectively. These coefficients give $\sigma_s^0 = 180–240$ bar and $\delta\sigma_s = 3–6$ bar if the normal stress is 300 bar. If we assume that its recovery rate can be linearly extrapolated to much longer time interval, the drop of the frictional strength C_d at the time of rupture would be about 25 per cent after 100 yr has elapsed. We tentatively use this as a starting value, but it was found that somewhat larger weakening rates are necessary to generate aftershocks in the case of high stress drops.

The rigidity, density and the shear wave velocity are assumed to be constant, but Poisson's ratio ν is varied between 0.20 and 0.30. This means that P wave velocity Vp takes values between 5.2–6.0 km/s for $Vs = 3.2$ km/s. For other parameters, we use almost the same values as in the main faulting (Mikumo & Miyatake 1978); grid spacing $h = \Delta x = \Delta y = 0.5$ km, fault length and width $2L = 2W = 20$ km, time increment $\Delta t = 0.05$ s, or $h = 1.0$ km, $2L = 2W = 40$ km, $\Delta t = 0.1$ s and $\Delta z = 1.0$ km. For numerical calculations of aftershock sequences, the time step has been taken as 30 min or 1 hr.

We have made a number of combinations of the above parameters, but only several representative cases are given in Table 1. Four examples of the distribution of static frictional strengths are also shown in Fig. 1(a)–(d). These distributions are similar in the previous paper. Case M-11 has a number of high strength inclusions exceeding 500 bar and hence is most heterogeneous. Case M-21 follows this example and Case M-31 has rather smaller inclusions with higher strengths. In Case M-41 the strengths are weakly non-uniform with an average of 250 bar and standard deviations of 25 bar.

4 Aftershock sequences

In this section, several results of numerical simulations for aftershock sequences are presented, and compared quantitatively with various observations.

4.1 SHEAR STRESS ON THE FAULT

Temporal variations in the shear stress at several selected segments on the fault, which have been calculated from equation (7) for Case M-11, are shown as an example in Fig. 2. The upper four diagrams show the stress behaviour on the segments that ruptured during the

Downloaded from http://gji.oxfordjournals.org/ at Library of Research Reactor Institute, Kyoto University on December 7, 2014

Table 1. Parameters specifying frictional fault model.

Model no.	Relaxation time (τ)	Relaxed coefficient (α)	Shear strength min–avr–max	Drop rate (C_d)	Inc. rate ($\delta\sigma_s$)
	min hr		bar		bar
11*	15–24	0.60–0.72	200–319–576	0.40	3.0
12*	15–24	0.66	200–319–576	0.40	3.0
13*	15–120	0.60–0.72	200–319–576	0.40	3.0
14	1	0.66	200–319–576	0.45	3.0
15	12	0.66	200–319–576	0.45	3.0
16	1–0.5	0.60–0.72	200–319–576	0.40	3.0
17	1–120	0.60–0.72	200–319–576	0.40	3.0
21*	15–24	0.66	200–306–590	0.40	3.0
31*	15–24	0.60–0.72	200–298–704	0.40	3.0
41*	15–24	0.60–0.72	200–280–365	0.45	3.0
42	15–24	0.60–0.72	200–280–365	0.40	3.0
51	15–24	0.60–0.72	200–330–841	0.40	3.0
61	15–24	0.60–0.72	200–237–481	0.40	3.0†
71	15–24	0.66	200–334–492	0.40	3.0†
111*	15–48	0.60–0.72	200–319–576	0.40	6.0

* Indicates the cases shown in the inserted figures.
† Initial stress is 205 bar. The cases without daggers have the initial stress of 198 bar.

main faulting. It can be seen that the initial stress of 200 bar drops to several tens of bar at the time of the main shock and then recovers with time, although their recovery rates are different, depending on the relaxation time assigned there. Small stress drops of the order of 10 bar or less occur during successive aftershocks, and minor step-like stress jumps take place due to the slip of adjacent segments. The lower four stresses indicate those on the unruptured fault segments. The concentrated stress is gradually relaxed in the right side case, and more slowly decreases after a slight jump in the second example. The first and third cases show sudden and large stress drops at the time of the largest aftershock that occurred within 1 hr. The latter examples suggest that aftershocks taking place in the unruptured regions would generally have a high stress drop comparable to that of the main faulting.

4.2 GENERAL PATTERN OF AFTERSHOCK SEQUENCES

The patterns given in the next three figures illustrate different types of space and time distributions of aftershocks. The fault dimension shown here is 40×40 km and the size of each segment is 1×1 km. The upper left in Figs 3 and 4 shows the final rupture front at the main faulting, and numerals on the left side of each step indicate the elapsed time after the main shock. In Fig. 3 (Case M-12), there remain rather wide unruptured regions on the left side. After a large aftershock (not shown here) followed the main faulting within 1 hr, a second moderate-size aftershock with high stress drops of about 100 bar takes place in this region, which was evidently initiated from the periphery of the stopped rupture front due to high stress concentration, and spread outside into the unruptured area. As time goes on to 4–6 hr later, several small unruptured segments also slip.

Downloaded from http://gji.oxfordjournals.org/ at Library of Research Reactor Institute, Kyoto University on December 7, 2014

Distribution of static frictional stress (×10 bar)
SFM = 200.0 SFD = 20.0 IS = 7777 DFM = 100.0 DFD = 0.0 ID = 555
Initial shear stress and its direction
STO = 200.0 bar DST = 0.0 deg DH = 1.00 BL = 40.0 BW = 40.0
DZ = 1.00 LC = 5
Distribution of velocities
VPM = 5.50 VSM = 3.20 DVD = 0.0 IV = 0 RHO = 2.75

M-11

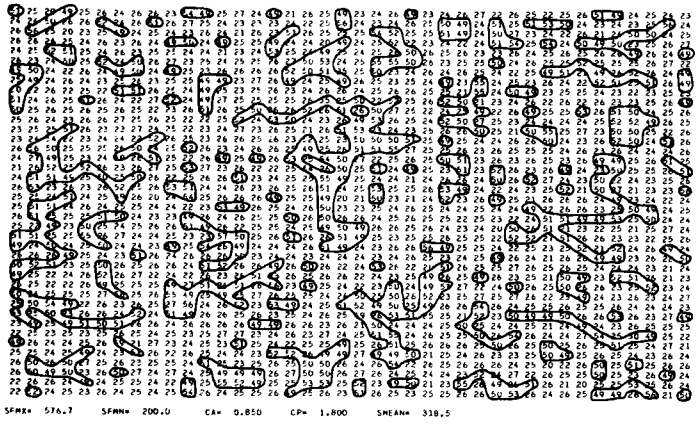

SFMX= 576.7 SFMN= 200.0 CA= 0.850 CP= 1.800 SMEAN= 338.5

M-31

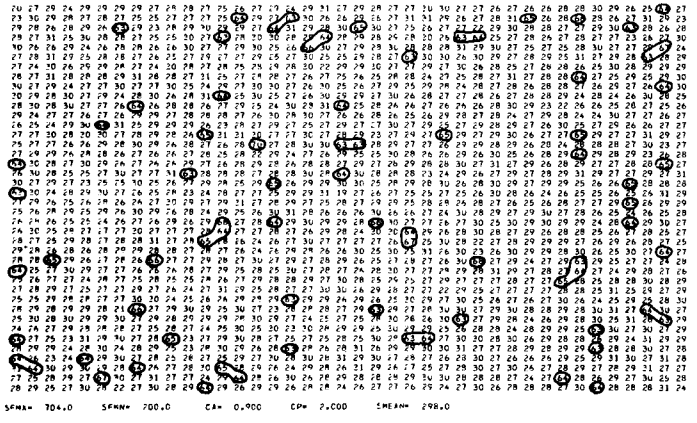

SFMX= 704.0 SFMN= 200.0 CA= 0.900 CP= 2.000 SMEAN= 298.0

Distribution of static frictional stress (×10 bar)
SFM = 200.0 SFD = 20.0 IS = 3000 DFM = 100.0 DFD = 0.0 ID = 555
Initial shear stress and its direction
STO = 198.0 bar DST = 0.0 deg DH = 1.00 BL = 40.0 BW = 40.0
DZ = 1.00 LC = 5
Distribution of velocities
VPM = 5.50 VSM = 3.20 DVD = 0.0 IV = 0 RHO = 2.75

M-21

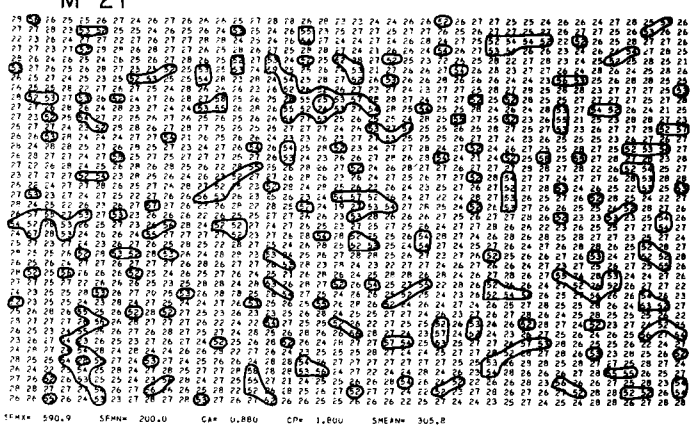

SFMX= 590.9 SFMN= 200.0 CA= 0.880 CP= 1.800 SMEAN= 305.8

M-41

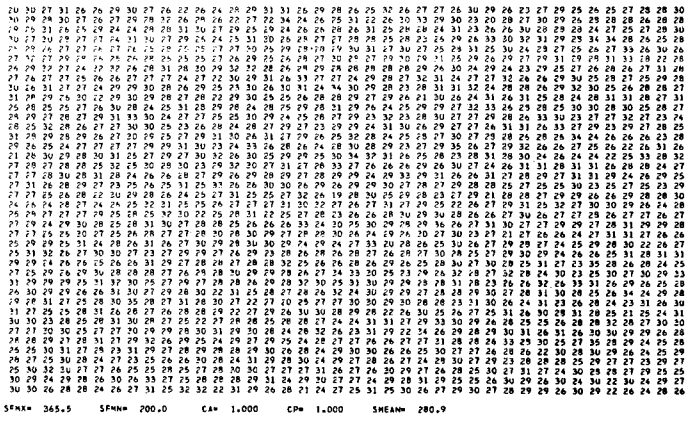

SFMX= 365.5 SFMN= 200.0 CA= 1.000 CP= 1.000 SMEAN= 280.9

Figure 1. Examples of the distribution of the static frictional strengths on the fault plane.

Downloaded from http://gji.oxfordjournals.org/ at Library of Research Reactor Institute, Kyoto University on December 7, 2014

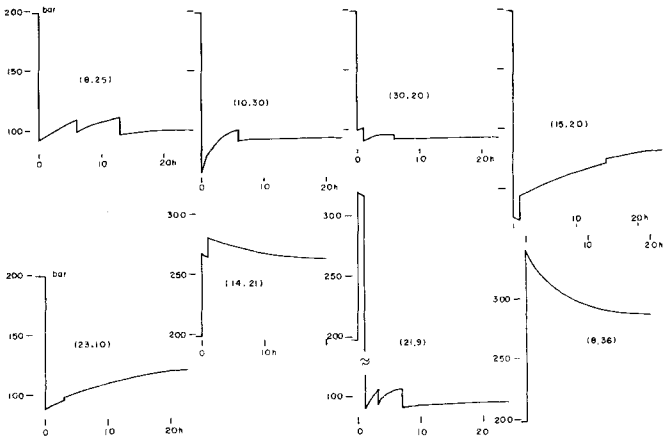

Figure 2. Time variations of the shear stress at several selected segments of the fault. Numerals in a bracket indicate the x- and y-coordinates of the segment.

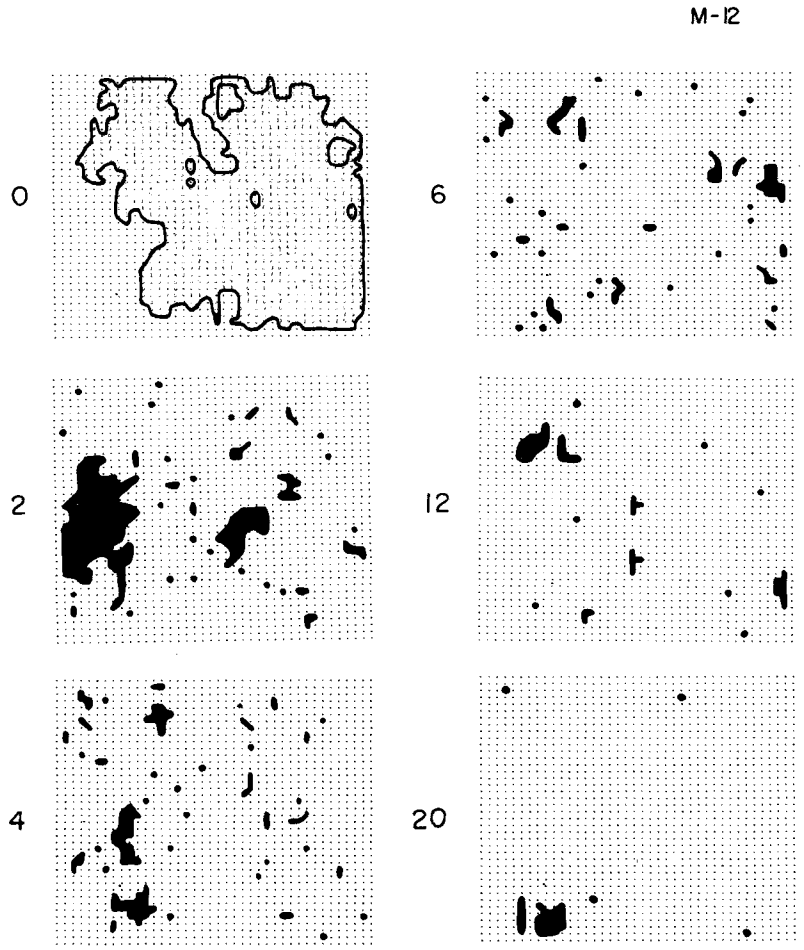

Figure 3. Space and time patterns of aftershocks for Case M-12. Numerals in the left-side of each time step indicate the elapsed time (in hr) after the main faulting. Fault dimension; 40 × 40 km, segment size; 1 × 1 km. (The same explanations apply to Figs 4, 5, 6 and 7.)

Downloaded from http://gji.oxfordjournals.org/ at Library of Research Reactor Institute, Kyoto University on December 7, 2014

Figure 4. Space and time patterns of aftershocks for Case M-31.

In Fig. 4 (Case M-31), the main rupture reached the prescribed fault boundary, leaving small unruptured segments inside. Small-size aftershocks take place 2 hr later around these segments, and one aftershock with low stress drop of 10 bar occurs 4 hr later in a rather wide region surrounded by the aftershocks at 2 hr. Several moderate-size aftershocks take place successively with time in spaced regions. Fig. 5 (Case M-41) gives an example in the case when the distribution of the frictional strength on the fault is weakly non-uniform and all segments of the fault have been ruptured at the time of the main shock. Only very small shocks occur 1 hr later. A large event at 8 hr appears to trigger four shocks at 9 hr in the surrounding regions and then to develop 10 hr later into the largest shock but with low stress drops of 10–15 bar. This type of sequence seems unlikely to occur in actual earthquakes, suggesting that the fracture strengths may be more heterogeneous than assumed here.

4.3 TEMPORAL VARIATIONS IN SPATIAL DISTRIBUTION OF AFTERSHOCKS

We investigate more closely temporal variations of spatial pattern of aftershocks with a time step of every 30 min or 1 hr after the main faulting up to 30 hr later.

Downloaded from http://gji.oxfordjournals.org/ at Library of Research Reactor Institute, Kyoto University on December 7, 2014

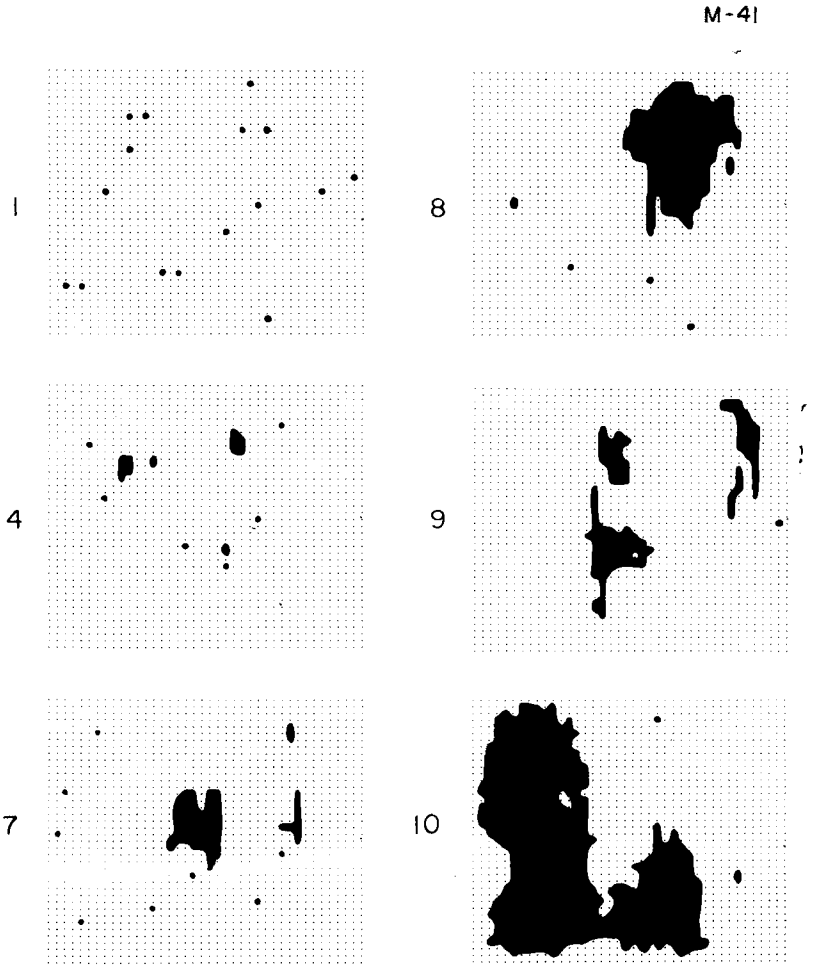

Figure 5. Space and time patterns of aftershocks for Case M-41.

Fig. 6(a) and (b) show one example, where there are again unruptured regions in the left-side and in a bay on the top. A large event with high stress drops of 70–100 bar, which might be called a multiple shock, occupies 1 hr later a major part of the unruptured regions, while several low-stress drop aftershocks take place in the ruptured area. It is obvious from this case together with Case M-12 that total aftershock area extends outside with time. This phenomena seems consistent with observations (e.g. Mogi 1968a). It may also be seen that fault segments successively slip after 1 hr to fill spaced gaps as time goes on. Aftershock activity gradually decays after 10 hr, and their stress drops, slip displacements and source areas appreciably decrease with time. The average stress drop and displacement for moderate-size aftershocks are about 15 bar and 10 cm, respectively.

Another example (Case M-21) is given in Fig. 7(a) and (b). The main faulting covered almost entire fault plane, but partly leaves small unruptured regions near the boundary. A moderate-size rupture initiates 1 hr later from the periphery of a small unruptured region on the left-top. The stress drop is again very large, exceeding 150 bar. We notice rather large number of wider-size aftershocks between 4 and 9 hr, as compared with Case M-11, which

Downloaded from http://gji.oxfordjournals.org/ at Library of Research Reactor Institute, Kyoto University on December 7, 2014

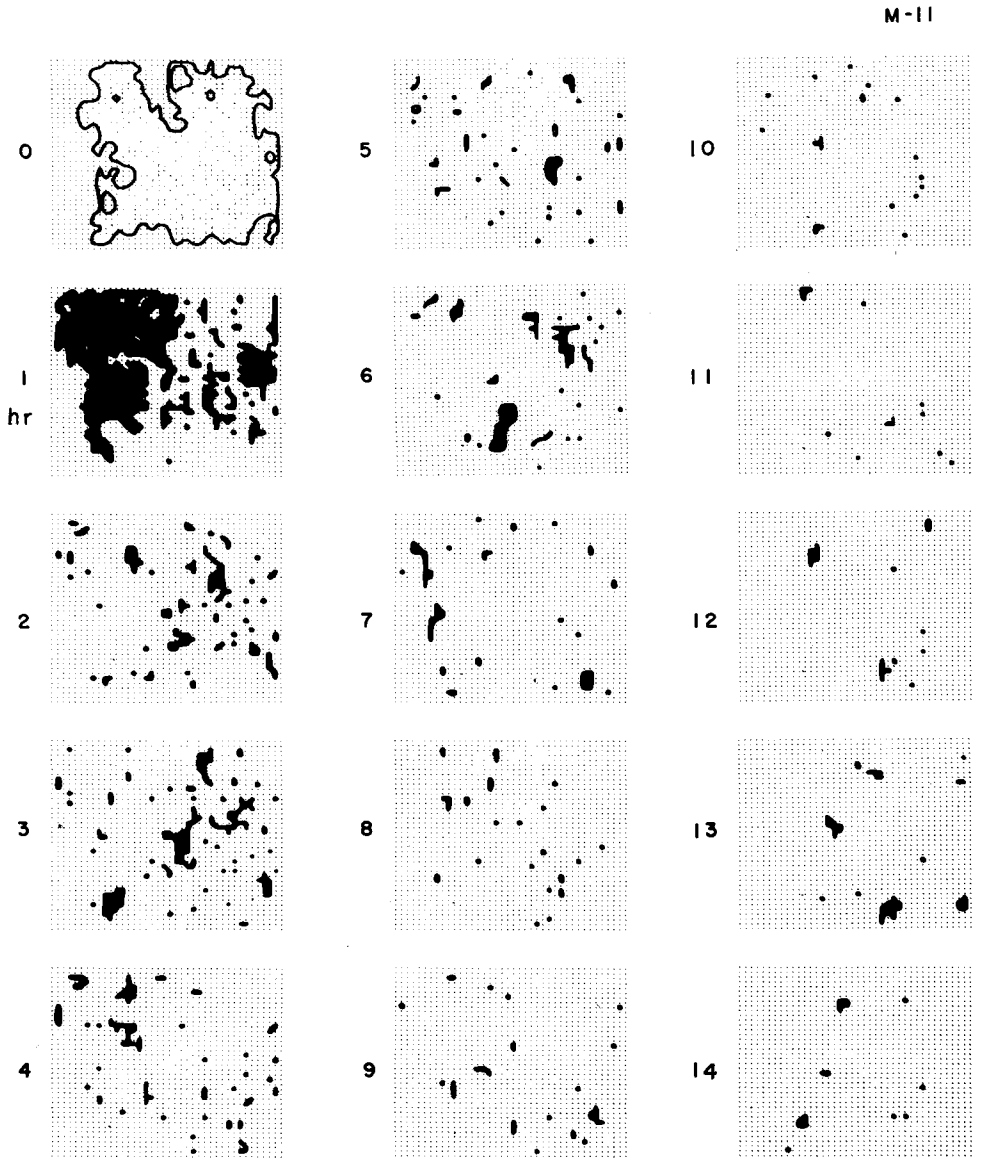

Figure 6. Temporal variations in the spatial distribution of aftershocks for Case M-11. Time step is taken every 1 hr.

have stress drops of the order of 20–30 bar. The number and source size of aftershocks gradually decrease after 10 hr, with intermittent occurrence of minor shocks. Fig. 7(c) shows the total area occupied by all aftershocks that occurred up to the indicated time. It is immediately noticed that the occupied area rapidly increases with time and almost covers the entire fault plane of the main shock within the time somewhat longer than the maximum relaxation time. Another important feature is that aftershocks at each time step generally take place in spaced regions so as to fill the gap which has not yet been ruptured after the

Downloaded from http://gji.oxfordjournals.org/ at Library of Research Reactor Institute, Kyoto University on December 7, 2014

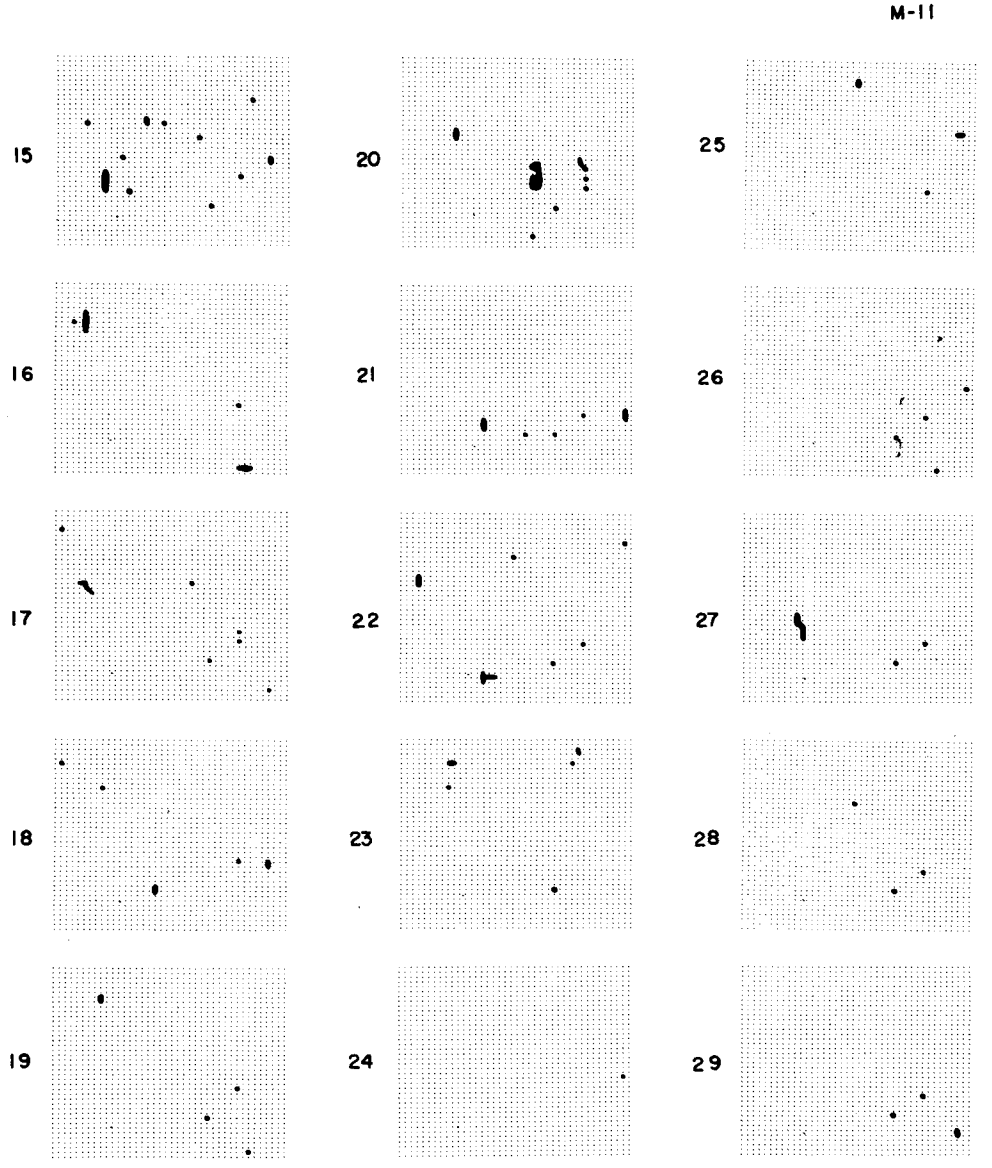

Figure 6 (b)

main faulting. These features might naturally be expected from re-adjustments of the shear stress on the fault plane.

4.4 STATISTICS OF AFTERSHOCK SEQUENCES

Some statistics of the simulated aftershock sequences are investigated in relation to the model parameters, and compared with that for observations. The frequency decay of aftershocks with time is shown for three different cases in Fig. 8(a), (b) and (c). It can be seen in the left-side of each figure that the number of aftershocks appears to decrease nearly in a

Downloaded from http://gji.oxfordjournals.org/ at Library of Research Reactor Institute, Kyoto University on December 7, 2014

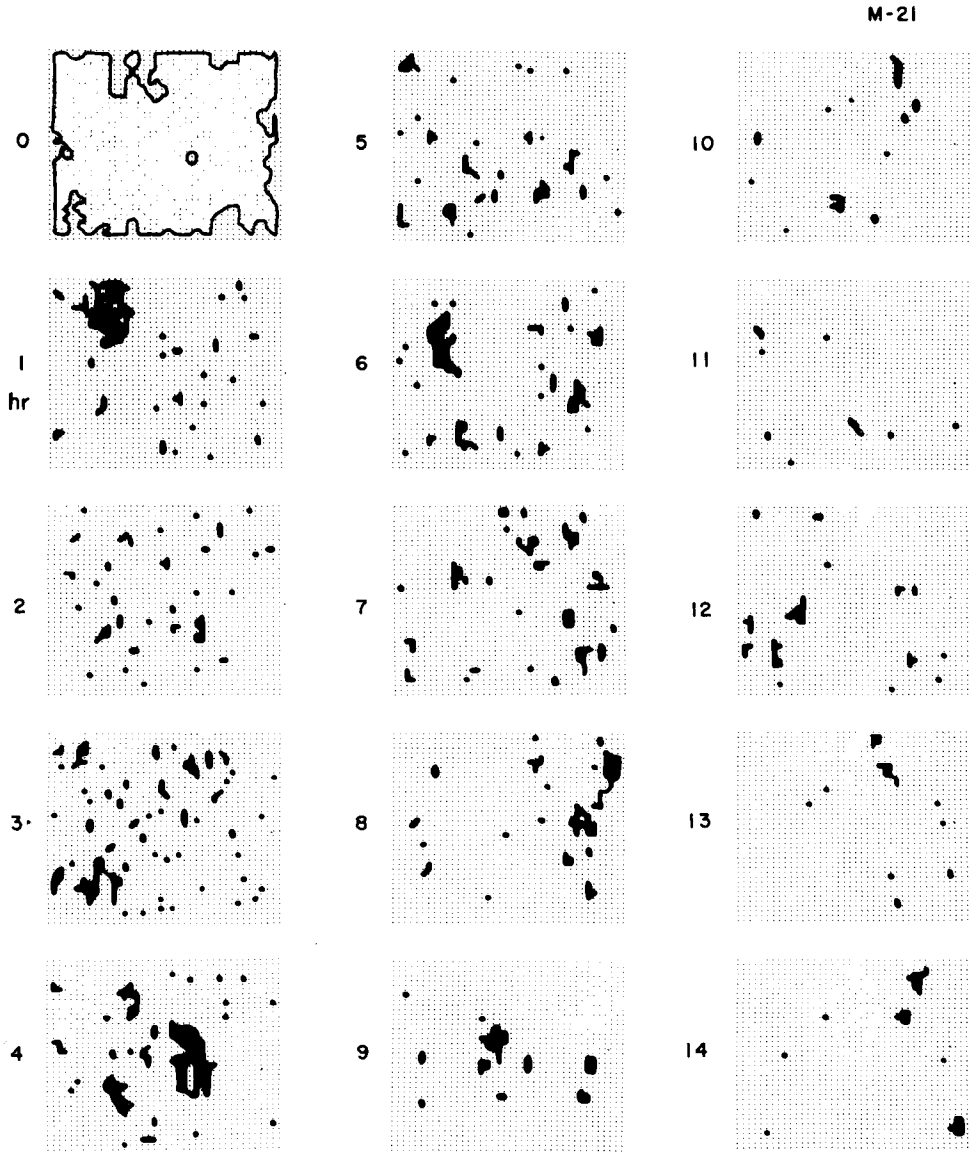

(a)

Figure 7. Temporal variations in the spatial distribution of aftershocks for Case M-21. Time step is taken every 1 hr.

hyperbolic form with some undulations. If these numbers at every 1 hr (in Cases M-11 and M-21) or every 3 hr (in Case M-13) are plotted in logarithmic scales, we have a nearly linear relation over the major part of the time interval except for very short and long ranges, as may be seen in the right-side. Slight downward deviations from the straight line around the longer time range may be due to the effects of the maximum relaxation time assigned here, which is 24 hr in Cases M-11 and M-21 and 120 hr (5 day) in Case M-13. The slope in the given three cases range between 1.1–1.4. Aftershock observations so far made indicate that

Downloaded from http://gji.oxfordjournals.org/ at Library of Research Reactor Institute, Kyoto University on December 7, 2014

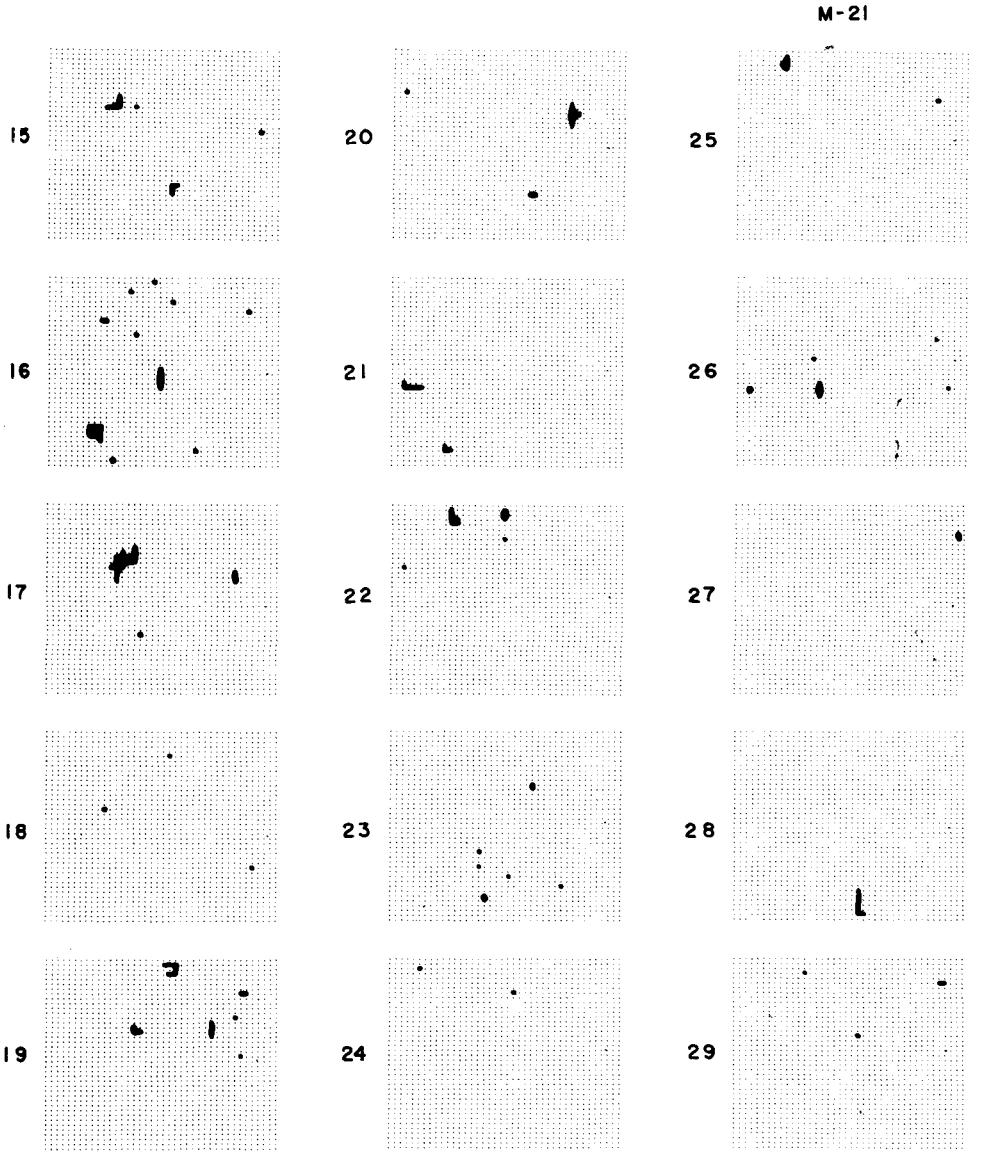

Figure 7 (b)

their decaying rate usually follows the form of $n(t) = A/(t + C)^p$ which is called Modified Omori's formula (Utsu 1961, 1970) where p and C are constants. p for a number of observations takes values between 1.0 and 1.5 (Utsu 1961, 1969; Mogi 1962a). The above formula has been derived from a probability theory by introducing fracture rates depending on time and location into a number of elementary areas in the aftershock source region (Utsu 1970). This concept is essentially similar to our model. In the fluid pore pressure model (Nur & Booker 1972; Booker 1974) the frequency decay is inversely proportional to the elapsed time, i.e. $C \cong 0$ and $p \cong 1$. The above numerical results from our model may well explain the above observations and also yields consistent results with the probability model and with the fluid flow model. It is to be noted that the constant decaying rate can be

Downloaded from http://gji.oxfordjournals.org/ at Library of Research Reactor Institute, Kyoto University on December 7, 2014

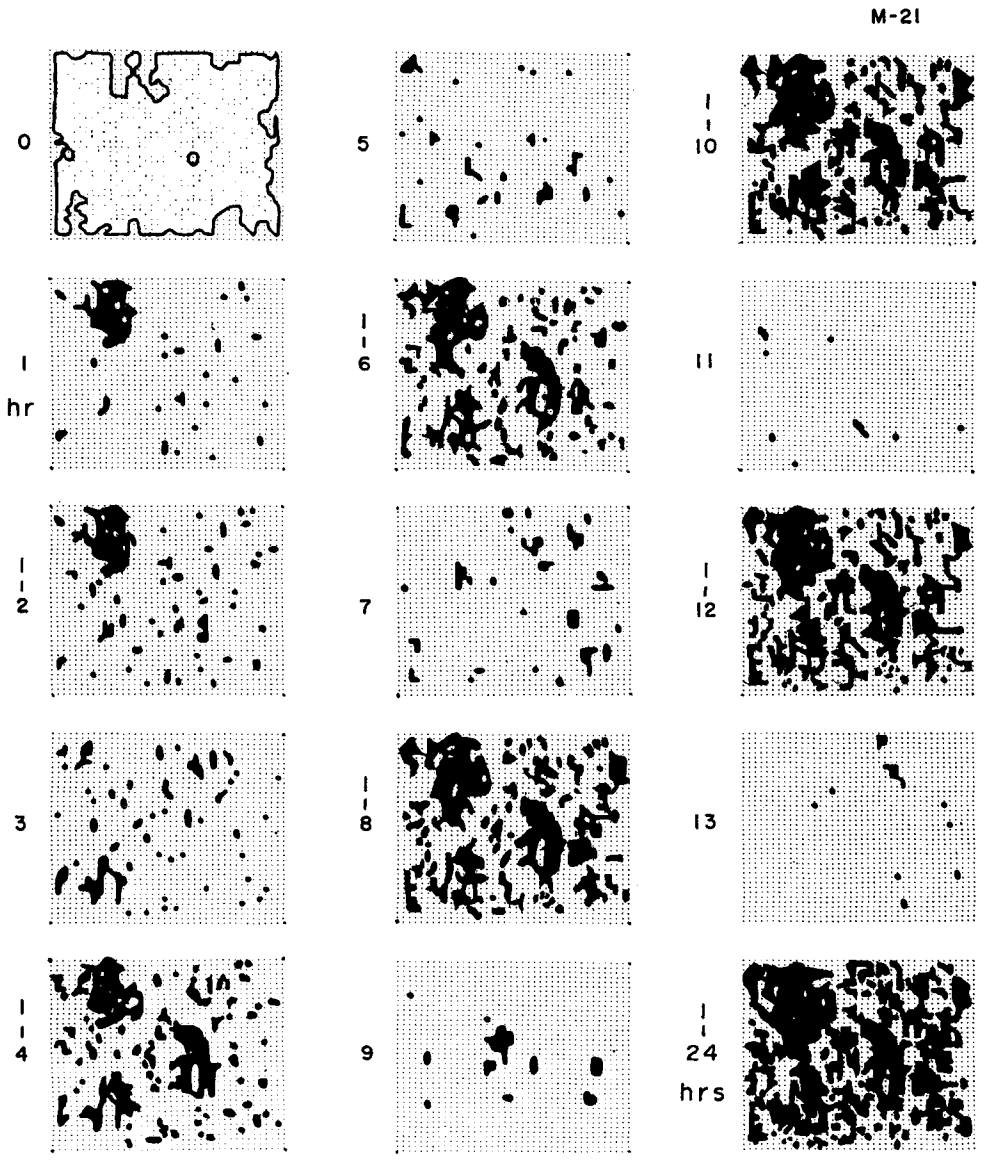

Figure 7 (c)

extended to 5 days or even longer so long as the relaxation times are uniform-randomly distributed up to the maximum value. However, if we assume a single constant relaxation time such as 1 hr (Case M-14), 12 hr (Case M-15), and 1 day or 5 day, the linearity can no longer hold. These results suggests that the relaxation time for fault gouge materials might take various values if the present viscoelastic relaxation mechanism is correct.

Fig. 9 shows the source area of aftershocks and their cumulative frequency plotted in logarithmic scales. The cumulative frequency is defined by

$$N(S) = \int_S^\infty n(S)\, dS,$$

Downloaded from http://gji.oxfordjournals.org/ at Library of Research Reactor Institute, Kyoto University on December 7, 2014

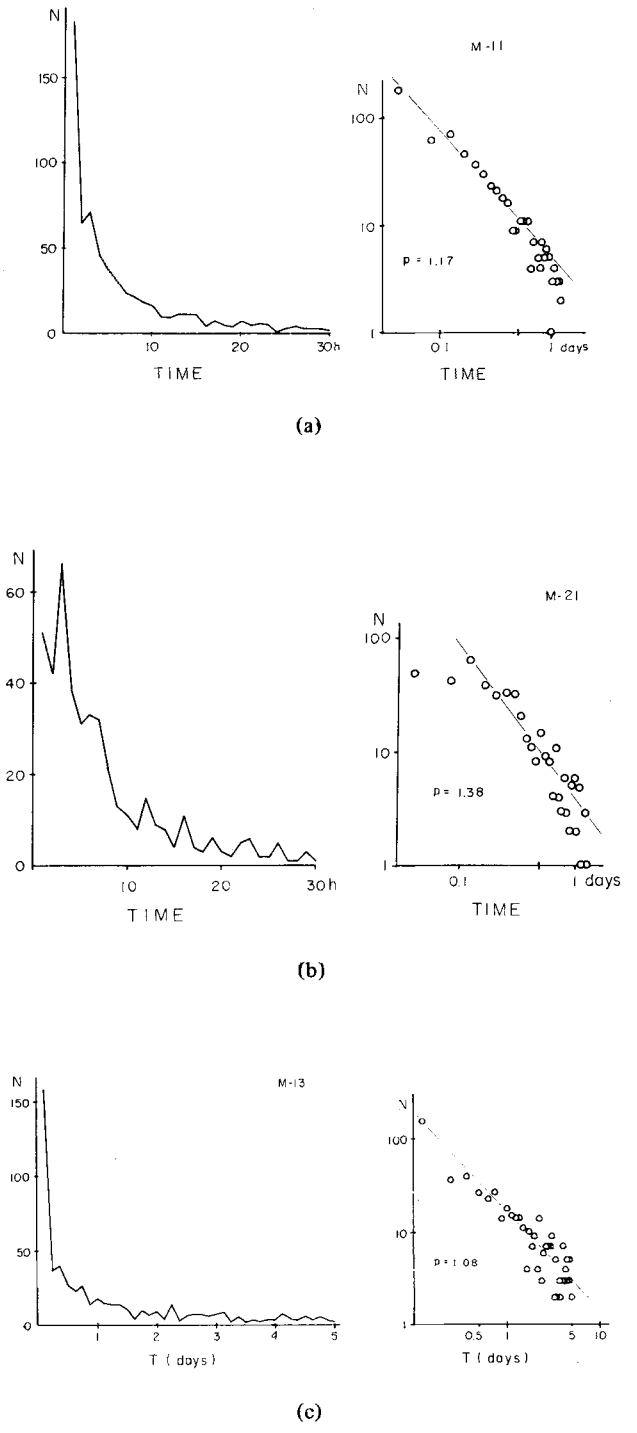

Figure 8. Frequency of aftershocks with time. Left: linear scale, right: logarithmic scale. (a) Case M-11, (b) Case M-21, (c) Case M-13.

Downloaded from http://gji.oxfordjournals.org/ at Library of Research Reactor Institute, Kyoto University on December 7, 2014

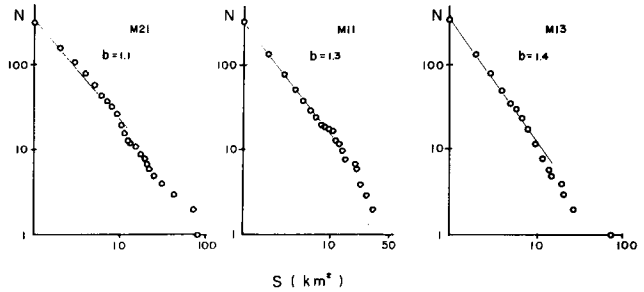

Figure 9. Source area–cumulative frequency relation of aftershocks in three different cases. b indicates the slope in $\log N$–$\log S$.

where $n(S)\,dS$ indicates the number of shocks with an area between S and $S+dS$. We immediately notice a good linear relation for all of the three cases shown here, with some minor fluctuations near the level of small numbers. A number of observational studies of major earthquakes (e.g. Kanamori & Anderson 1975) and aftershocks (e.g. Utsu & Seki 1955; Utsu 1961, 1969) has shown that there is a proportionality between the magnitude of earthquakes and its source area, i.e. $M \sim \log S$. If we combine this relation with the above results, the slope in $\log N \sim \log S$ should give the well-known b-value. The slope ranging from 1.1 to 1.4 shown in Fig. 9 seems somewhat larger than those observed over the world (e.g. Utsu 1971).

In the present study, the fault displacements can be calculated for each segment of the aftershock source area, and hence the seismic moment can also be evaluated by definition from

$$M_0 = \iint \mu D(x, y)\, dx\, dy$$

for each shock. The seismic moments thus obtained for the main faulting and the second (or third) largest shock in Case M-11 are 1.9×10^{26} and 4.6×10^{25} (or 5.3×10^{24}) dyne cm, and in Case M-21, 2.5×10^{26} and 3.6×10^{24} dyne cm, respectively. If the magnitude is proportional to $\log M_0$, the difference in the magnitude between the main shock and the largest aftershock would be 0.6 (or 1.5) in Case M-11 and 1.8 in Case M-21. The first one seems too

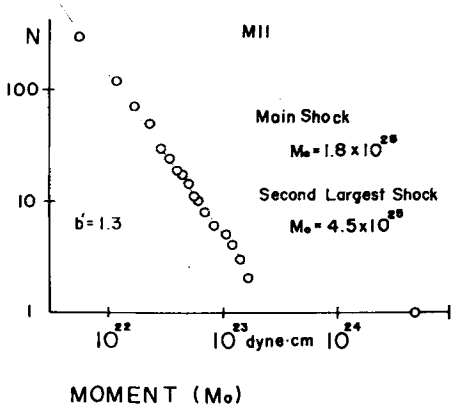

Figure 10. Seismic moment–cumulative frequency relation of aftershocks in Case M-11. b' indicates the slope in $\log N$–$\log M_0$.

Downloaded from http://gji.oxfordjournals.org/ at Library of Research Reactor Institute, Kyoto University on December 7, 2014

small, indicating that the second largest shock in Case M-11 should be called a multiple event rather than the largest aftershock as mentioned in Fig. 6(a). If this is excluded, the magnitude difference in both cases appears consistent again with observations (Utsu 1961, 1969). In Fig. 10, the seismic moments calculated for all aftershocks except for the multiple event are plotted against their cumulative frequency

$$N(M_0) = \int_{M_0}^{\infty} n(M_0)\, dM_0.$$

There is again a linear relation between them, and the slope gives the same value of 1.3 as that in the $\log N$–$\log S$ relation in Case M-11. This indicates that the seismic moment M_0 is proportional to $\log S$ in our model, and appears to give indirect support to the empirical relations $M \sim \log M_0 \sim \log S$ (Utsu 1961; Kanamori & Anderson 1975).

One reason for the estimated b-value slightly larger than those in the observations might be attributed partly to the present quasi-three-dimensional model with a fixed boundary (Mikumo & Miyatake 1978) which would yield smaller fault displacements as compared with those in an infinite medium. However, this effect should be commonly included in all calculated displacements and hence the slope would not be greatly changed.

Several natures of aftershock sequences are further discussed on the basis of numerical experiments together with some qualitative considerations. In the present model, the occurrence of aftershocks should be controlled by the relative magnitude of the shear stress with respect to the frictional strength. The relative levels are mainly governed by a coefficient of the recovered stress α and the weakening rate of the strength C_d. If α and/or C_d are too large, the shear stress cannot overcome the frictional strength, and no slips or aftershocks would be generated. For small values of α and/or C_d, the stress right after the main faulting exceeds the strength on all fault segments, and hence a large faulting immediately takes place over the entire fault. This implies that a dimensionless factor $C_d/(1-\alpha)$ specifies the absolute number of aftershocks.

The decaying rate of aftershocks with time, p, depends on the recovery rate $\delta\sigma_s$ of the frictional strength relative to the relaxation time τ of the shear stress. If $\delta\sigma_s$ increases for a certain distribution of τ, the number of aftershocks rapidly decreases with time and hence p becomes larger. However, p does not change greatly for longer maximum relaxation time with a constant $\delta\sigma_s$, as can be seen in Cases M-11 and M-13 in Fig. 8(a) and (c). Furthermore, a comparison in the distributions of the frictional strength in Fig. 1 indicates that more heterogeneous faults such as in Case M-11 gives a smaller value of p than in Case M-21. This is because it takes longer time to complete re-adjustments of the shear stress distribution over the fault.

The b-value for aftershock sequences may be affected by the dynamical rupture process of each aftershock, depending on how easily the source area could be extended. This naturally depends on the distribution of the frictional strengths, and is not seriously affected by other parameters. Figs 9 and 10 together with some other results not shown here reveal that more heterogeneous strengths yield large numbers of smaller aftershocks and hence lead to larger b-values. These natures seem consistent with the results from laboratory experiments on microfracturing in rock material (e.g. Mogi 1962b) and also with some aftershock observations in different crustal regions (e.g. Mogi 1963). Further numerical calculations show that if dynamic frictional strengths are not constant but weakly non-uniform in proportion to the static strengths, b tends to be small (Miyatake 1979, in preparation). This trend may be explained by the effects of reducing heterogeneities of the stress drops and of the resulted shear stresses.

Downloaded from http://gji.oxfordjournals.org/ at Library of Research Reactor Institute, Kyoto University on December 7, 2014

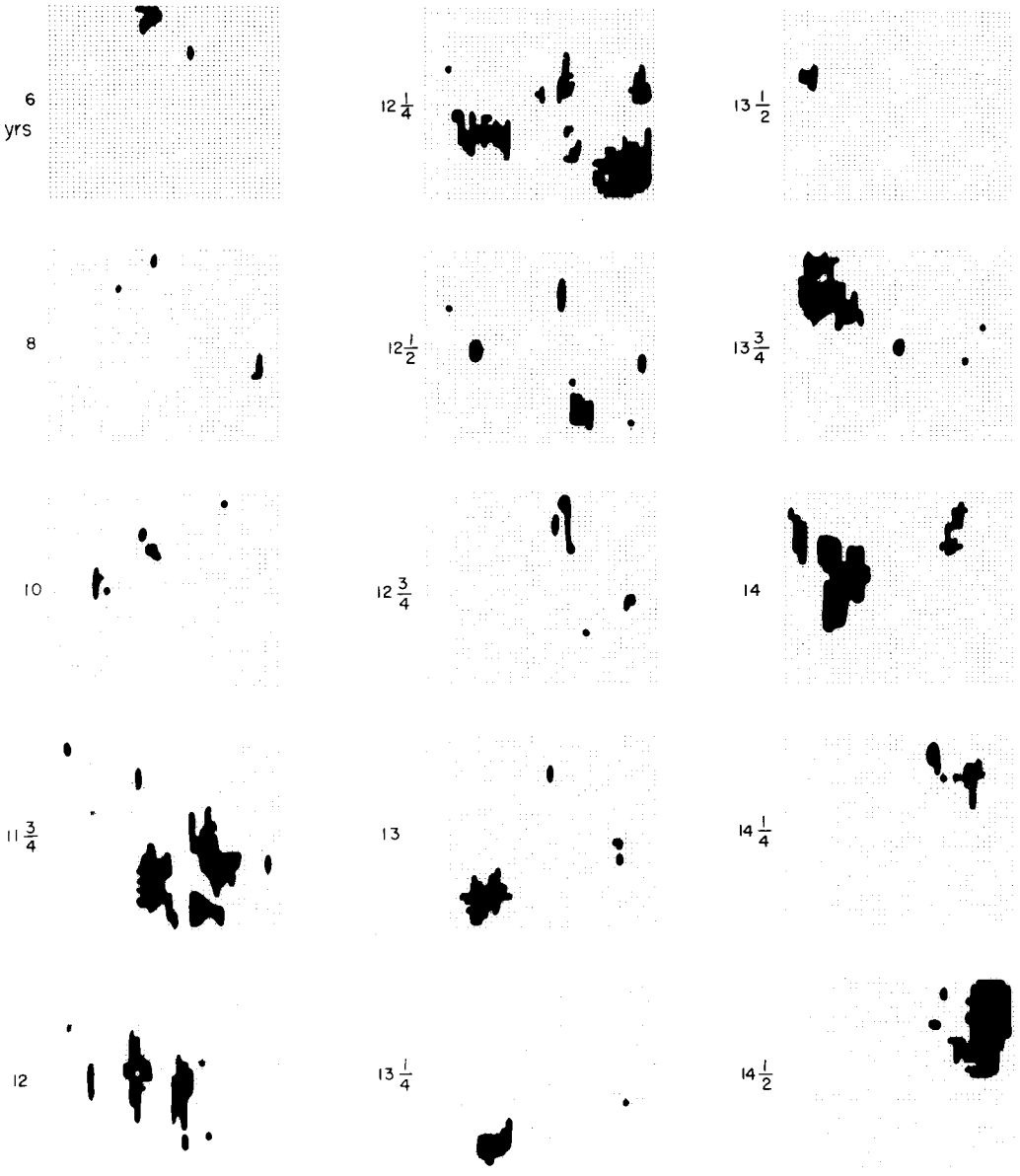

Figure 11. Space and time patterns of major shocks in the time range up to 25 yr. Time step is indicated by yr. (Case M-111 slightly modified from M-11.)

5 Recurrence of major shocks

It would be interesting to see if coming foreshocks and major shocks repeatedly occur on the present frictional fault during a long time range in a future, after the aftershock sequences have ceased. Aftershock activity gradually decays and finally ceases when the shear stress distribution has been re-adjusted and goes down below the level of the fracture strength on all segments of the fault. The only conceivable driving force that could generate

Downloaded from http://gji.oxfordjournals.org/ at Library of Research Reactor Institute, Kyoto University on December 7, 2014

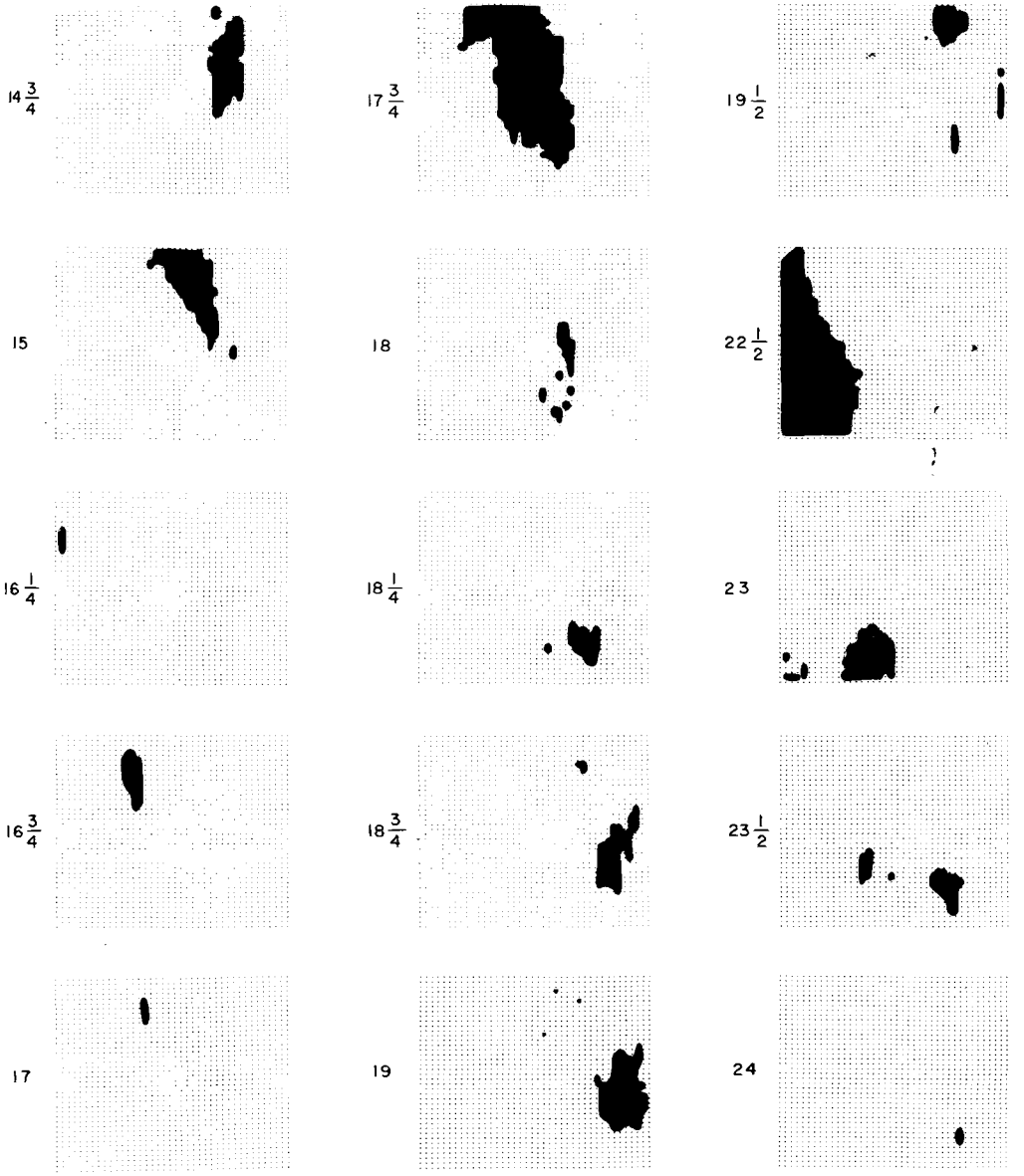

Figure 11 (b)

future shocks on the same fault would be increasing tectonic shear stress which may result from the drag force of plate movements. This effect has been taken into consideration as $\alpha C_k(t - T_1)$ in equation (7). The increasing rate of the force C_k is related to the relative velocity $\dot{U}$ of plate movements as mentioned before. Since the velocity is of the order of $\dot{U} = 2 - 10$ cm/yr for interplate fault planes, but would be much less than that for intraplate faults, we take several values between 0.3--3.0 cm/yr, which yields the stress change of $\dot{\sigma} = 1 - 10$ bar/yr. The smaller rate seems consistent with secular strain observations with the order of several μ strains.

Similar calculations are continued under the increasing tectonic stress up to the time scale of 30 yr after a 36-hr aftershock sequence. The time increment has been taken as 1 yr in a

Downloaded from http://gji.oxfordjournals.org/ at Library of Research Reactor Institute, Kyoto University on December 7, 2014

first surveying trial, and subdivided successively back into finer intervals, 1/2, 1/4, 1/8 and 1/12 yr. This is because the stress accumulated during a long time interval would break larger areas on the fault, if a widely spaced time increment is used. Preliminary calculations show that in most cases an interval of 1/4 yr or sometimes 1/8 yr is accurately enough to see the rupture pattern for 30 yr. Fig. 11(a) and (b) illustrates temporal variations in the spatial pattern of major shocks mostly at every 1/4-yr interval, where $\dot{U}$ is taken as 0.5 cm/yr. Most of other parameters are fixed as in the aftershock calculation for Case M-11, except that $\tau_{max} = 2$ day and $\delta\sigma_s = 6$ bar. In these figures, if the indicated time is skipped to longer than 1/4 yr, no earthquakes actually take place during this period, and small shocks that occurred at intervals shorter than 1/4 yr are tentatively superposed at the next time step. Fig. 12 shows the number of shocks that occurred within 25 yr (lower) and of their accumulated seismic moment (upper). The latter comes from a simple summation of the seismic moment for each shock which has been evaluated in the same way as in the case of aftershocks. This may be regarded as the total strain energy released at the specified period. The approximate magnitudes converted from the accumulated moments by an empirical formula (Aki 1972) are indicated for the sake of reference at the left-end.

Close investigations with Figs 11 and 12 reveal some interesting features of future earthquake sequences. The first to be noted for this example is a complete silent period up to 6 yr after the main faulting and its aftershock sequence, excepting only one very small shock at 2 yr, as may be understood from Fig. 12. This is the period for which the once dropped and recovering shear stress does not yet reach the level of the frictional strength. Fig. 11(a) shows that small shocks emerge 6 yr later and take place sporadically at 8, 10 and 10.5 yr, but their activity is still low. These shocks might be regarded as foreshocks to a succeeding activity. The first active period starts at 11.75 yr and continues to 15 yr later, during which larger shocks with stress drops of 40–80 bar occur successively, as seen from Fig. 12. The rupture pattern shown in Fig. 11(a) appears rather randomly distributed particularly between 11.75 and 13.25 yr, but closer examinations indicate that all these shocks take place successively in adjacent spaced regions as in the case of aftershocks. Similar phenomena have been suggested in the simple mechanical model of Otsuka (1972). These shocks after 13.5 yr appear to move from the left-top to the right-side in Fig. 11(a), and this activity ceases with a large shock having stress drops of about 100 bar at 15 yr. There is a period of low activity between 15 and 17 yr, but small shocks during this period may again be foreshocks to the second largest shock at 17.75 yr, which has stress drops exceeding 100 bar. It is interesting to see again in Fig. 11(b) that the second high activity lasting to 19 yr clearly indicate migrations from the left-top to the right-bottom over about 50 km within 2.5 yr. This speed may probably be associated with the increasing rate of

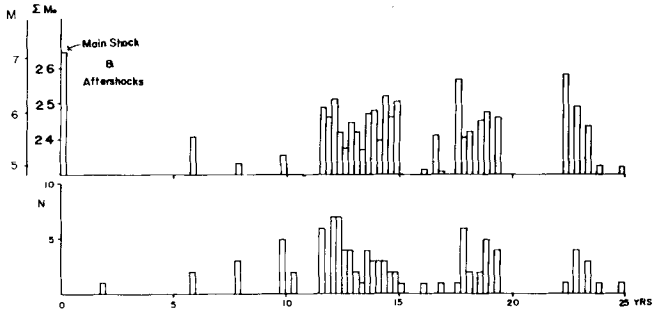

Figure 12. Time sequence of major shocks over 25 yr. Upper: accumulated seismic moment (ΣM_0 in logarithmic scale, units in dyne cm) against time; lower: number of shocks against time.

Downloaded from http://gji.oxfordjournals.org/ at Library of Research Reactor Institute, Kyoto University on December 7, 2014

the shear stress and also with the recovery rate of the frictional strength but not certain at this moment. The succeeding 3 yr is the period of complete silence, which may be termed as seismic time-gap, as is clear from Fig. 12. After this period the largest shock with stress drop of about 120 bar and seismic moment of 5.6×10^{25} dyne cm suddenly takes place in a spaced region which has not been ruptured since 14 yr and may be regarded as seismic space-gap. The third activity also shows a sort of migration and ceases at 25 yr. The above patterns would be somewhat changed if we take different parameters.

Nevertheless, the important features revealed from the foregoing calculations are the very low activity sometimes with a small number of foreshocks or the complete time-gap prior to a large shock, the successive ruptures of space-gaps, and the slow migration of seismic activity, although all these are the phenomena on a single fault surface. However, if this fault plane could be extended and applied to an extensive region such as in plate boundaries along oceanic trenches, it might be possible to compare these phenomena with various observations. Precursory time gaps to a large earthquake, which is preceded by foreshock activity in its surrounding regions, have been reported for several cases (e.g. Mogi 1969; Evison 1977; Ishida & Kanamori 1978). It has been also found that large seismic space-gaps for interplace earthquakes along oceanic trenches were successively ruptured in a long time interval (e.g. Mogi 1968b; Kelleher, Sykes & Oliver 1973; Kelleher & Savino 1975; Utsu 1974). Local southward migration of seismic activity along the Japan trench and global clockwise migration of great earthquakes along the circum-Pacific belt have also been reported (Mogi 1968c, d). There is a possibility that these observed earthquake phenomena might be partially explained by some physical models similar to the present type of frictional faults with non-uniform strengths under inhomogeneous stress. However, the results we have shown here are only preliminary and await more studies before reaching a conclusion.

6 Some additional remarks

The present model has been introduced to approximate the viscoelastic behaviours of rock or gouge materials on the fault surface, which are due to various processes such as creep, fluid flow and consolidation. It has been shown in the foregoing sections that the uniform-randomly distributed relaxation times up to several days could account for the hyperbolic decay of aftershocks with time over the same period. It is found, however, (e.g. Utsu 1969) that aftershock activity following some great earthquakes decays with time-invariant rates p even over several tens of years. There is also some experimental evidence (e.g. Itô 1974) that the relaxation time for long-term creep of virgin rocks could reach 100 yr. If we take into consideration these data, the present model would have to be somewhat modified. An alternative would be the standard linear solid which is connected in series to another Maxwell element with much longer relaxation times. For this model, we have a relationship corresponding to equation (3), which can be solved in a similar way. In this case, however, the stress recovery due to this relaxation mechanism would be coupled to the increasing tectonic stress over a long time range and could have some effect on the time and space patterns of earthquake sequences.

Another possible mechanism for aftershock sequences would be time-delayed stress corrosion or weakening of the fracture strength due to concentrated stress (e.g. Mogi 1962b; Scholz 1968; Knopoff 1972; Anderson & Grew 1977), which is similar to static fatigue or creep failure under a constantly applied stress. In this model, the time sequence of after-shocks depends primarily on a time-dependent weakening of the strength. From laboratory experiments on microfracturing of rocks, this weakening effect has been expressed in a form

Downloaded from http://gji.oxfordjournals.org/ at Library of Research Reactor Institute, Kyoto University on December 7, 2014

(Mogi 1962b; Scholz 1968), $\mu(t) = (1/k) \exp[-\beta\{\sigma(t) - S\}]$, whereas a simpler form has been used in a one-dimensional simulation, $df/dt = -\{\sigma(t) - S\}/\tau$ (Rundle & Jackson 1977). $\mu(t)\,dt$ is the transition probability of fracture and may be related to the weakening rate of the fracture strength df/dt and the mean time to fracture $\langle t \rangle$ as $\mu(t)\,dt = 1/\langle t \rangle = df/dt$. $\sigma(t)$ and S are the stress and the ultimate strength and β, k and τ are constants. It has been shown from the above empirical formula (Scholz 1968) that the number of shocks decreases inversely proportional to the elapsed time over appropriate time intervals.

In our present fault model, high stress concentration remains after the main faulting around some unruptured regions with high strengths. If we consider the above effects of stress corrosion, all of these unruptured regions would soon break at an early stage after the main shock. The concentrated stress rapidly drops to the level of the dynamic frictional strength and would be smoothed out. After this time there would be almost no succeeding shocks taking place *on* the fault plane, unless the shear stress due to increasing tectonic loading could exceed again the fracture strength. From these considerations, the stress corrosion mechanism could generate aftershocks *around* the fault edges where high stresses are still concentrated, but may not be a predominant candidate to account for various processes *on* the fault plane.

7 Conclusions

We have investigated the space and time characteristics of earthquake sequences on a three-dimensional frictional fault model, which has non-uniform frictional strengths and relaxation times and is subjected to a time-dependent shear stress, in a standard viscoelastic solid. In this model, aftershocks and the recurrence of major shocks in a long time range take place as dynamical ruptures on the fault, when the recovering shear stress after the main faulting exceeds a time-dependent fracture strength. The main conclusions we obtained are as follows:

(1) Aftershocks take place successively in spaced regions on the fault so as to fill the gaps which have not yet been ruptured since the main shock, and sometimes in the regions left unruptured during the main faulting. The aftershock area used to extend outside with time, and finally covered almost the entire fault plane within a time somewhat longer than the maximum relaxation time. Aftershocks taking place in the unruptured regions have high stress drops comparable to that of the main faulting, while those in the ruptured regions have low stress drops due to minor readjustments of the shear stress.
(2) The frequency decay of aftershocks with time follows a hyperbolic law with its exponent p ranging between 1.1–1.4, which may well explain a number of observations. The decaying rate p becomes smaller for more heterogeneous distribution of frictional strength on the fault, and larger for more rapid recovery of the weakened strength after the main faulting. A good linear relation holds for the source area–cumulative frequency and also for the seismic moment–cumulative frequency of the generated aftershocks. The b-value estimated from the relations are slightly larger than that from observations, but these are affected by fault properties. More heterogeneous frictional strengths give larger b-values.
(3) There is a completely silent period of seismic activity before the recurrence of major shocks, after a sequence of aftershocks has ceased. The coming major shocks take place with high stress drop, successively in adjacent spaced gap regions and sometimes show slow-speed migration. The largest shocks in a series of activity are sometimes preceded by a complete time-gap or very low activity with a small number of foreshocks.

The present frictional fault model provides some explanations to various observed phenomena on a sequence of earthquakes.

Downloaded from http://gji.oxfordjournals.org/ at Library of Research Reactor Institute, Kyoto University on December 7, 2014

Acknowledgments

We would like to thank Professors Keiiti Aki, Tomowo Hirasawa and Hidebumi Itô and the staff members of our laboratory for several discussions and comments. The computations were made at the Data Processing Center of Kyoto University and at the Computer Room of the Institute for Chemical Research, Kyoto University, Uji.

References

Aki, K., 1972. Scaling law of earthquake source time function, *Geophys. J. R. astr. Soc.*, **31**, 3–25.

Anderson, O. L. & Grew, P. C., 1977. Stress corrosion theory of crack propagation with applications to geophysics, *Rev. Geophys.*, **15**, 77–104.

Benioff, H., 1951. Earthquakes and rock creep, *Bull. seism. Soc. Am.*, **41**, 31–62.

Booker, J. R., 1974. Time dependent strain following faulting of a porous medium, *J. geophys. Res.*, **79**, 2037–2044.

Cohen, S. C., 1977. Computer simulation of earthquakes, *J. geophys. Res.*, **82**, 3781–3796.

Das, S. & Aki, K., 1977. Fault plane with barriers: A versatile earthquake model, *J. geophys. Res.*, **82**, 5658–5670.

Dieterich, J. H., 1972a. Time-dependent friction in rocks, *J. geophys. Res.*, **77**, 3690–3697.

Dieterich, J. H., 1972b. Time-dependent friction as a possible mechanism for aftershocks, *J. geophys. Res.*, **77**, 3771–3781.

Dieterich, J. H., 1978. Time-dependent friction and the mechanics of stick–slip, *Pure appl. Geophys.*, **116**, 790–806.

Engelder, J. T., Logan, J. M. & Handin, J., 1975. The sliding characteristics of sandstone on quartz fault gouge, *Pure appl. Geophys.*, **113**, 69–86.

Evison, F. F., 1977. The precursory earthquake swarm, *Phys. Earth planet. Interiors*, **15**, 19–23.

Ishida, M. & Kanamori, H., 1978. The foreshock activity of the 1971 San Fernando earthquake, California, *Bull. seism. Soc. Am.*, **68**, 1265–1279.

Israel, M. & Nur, A., 1979. A complete solution of a one-dimensional propagating fault with nonuniform stress and strength, *J. geophys. Res.*, **84**, 2223–2234.

Itô, H., 1974. Long-term creep of rocks, in *Flow of Solids* (in Japanese), Tokai University Press.

Itô, H. & Sasajima, S., 1979. Long-term creep experiment of rocks for 4 years, *Rock Mech. Japan*, **3**, in press.

Kanamori, H. & Anderson, D. L., 1975. Theoretical basis of some empirical relations in seismology, *Bull. seism. Soc. Am.*, **65**, 1073–1095.

Kelleher, J. & Savino, J., 1975. Distribution of seismicity before large strike slip and thrust-type earthquakes, *J. geophys. Res.*, **80**, 260–271.

Kelleher, J., Sykes, L. R. & Oliver, J., 1973. Possible criteria for predicting earthquake locations and their application to major plate boundaries of the Pacific and the Caribbean, *J. geophys. Res.*, **78**, 2545–2585.

Knopoff, L., 1972, Model for aftershock occurrence, in *Flow and Fracture of Rocks*, pp 259–263, Geophys. Monog. **16**, Am. Geophys. Union.

Knopoff, L., Mouton, J. O. & Burridge, R., 1973. The dynamics of a one-dimensional fault in the presence of friction, *Geophys. J. R. astr. Soc.*, **35**, 169–184.

Liu, H., Anderson, D. L. & Kanamori, H., 1976. Velocity dispersion due to anelasticity; Implications for seismology and mantle composition, *Geophys. J. R. astr. Soc.*, **47**, 41–58.

Lomnitz, C., 1956. Creep measurements in igneous rocks, *J. Geol.*, **64**, 473–479.

Mikumo, T. & Miyatake, T., 1978. Dynamical rupture process on a three-dimensional fault with non-uniform frictions, and near-field seismic waves, *Geophys. J. R. astr. Soc.*, **54**, 417–438.

Miyatake, T., 1977. Numerical simulation of dynamical rupture process (in Japanese), *ZISIN*, Ser. II, **30**, 449–461.

Miyatake, T., 1978. Numerical simulation of aftershock process (in Japanese), *ZISIN*, Ser. II, **31**, 161–177.

Mogi, K., 1962a. On the time distribution of aftershocks accompanying the recent major earthquakes in and near Japan, *Bull. Earthq. Res. Inst. Tokyo Univ.*, **40**, 107–124.

Mogi, K., 1962b. Study of elastic shocks caused by the fracture of heterogeneous materials and its relations to earthquake phenomena, *Bull. Earthq. Res. Inst. Tokyo Univ.*, **40**, 125–173.

Downloaded from http://gji.oxfordjournals.org/ at Library of Research Reactor Institute, Kyoto University on December 7, 2014

Mogi, K., 1963. Some discussions on aftershocks, foreshocks and earthquake swarms – the fracture of a semi-infinite body caused by an inner stress origin and its relation to the earthquake phenomena (third paper), *Bull. Earthq. Res. Inst. Tokyo Univ.*, **41**, 615–658.

Mogi, K., 1968a. Development of aftershock areas of great earthquakes, *Bull. Earthq. Res. Inst. Tokyo Univ.*, **46**, 175–203.

Mogi, K., 1968b. Some features of recent seismic activity in and near Japan (1), *Bull. Earthq. Res. Inst. Tokyo Univ.*, **46**, 1225–1236.

Mogi, K., 1968c. Migration of seismic activity, *Bull. Earthq. Res. Inst. Tokyo Univ.*, **46**, 53–74.

Mogi, K., 1968d. Sequential occurrence of recent great earthquakes, *J. Phys. Earth*, **16**, 30–36.

Mogi, K., 1969. Some features of recent seismic activity in and near Japan (2) – Activity before and after great earthquakes, *Bull. Earthq. Res. Inst. Tokyo Univ.*, **47**, 395–417.

Nur, A., 1978. Nonuniform friction as a physical basis for earthquake mechanics, *Pure appl. Geophys.*, **116**, 964–989.

Nur, A. & Booker, J. R., 1972. Aftershocks caused by pore fluid flow? *Science*, **175**, 885–887.

Otsuka, M., 1972. A simulation of earthquake occurrence, *Phys. Earth planet. Interiors*, **6**, 311–315.

Rundle, J. B. & Jackson, D. D., 1977. Numerical simulation of earthquake sequences, *Bull. seism. Soc. Am.*, **67**, 1363–1377.

Savage, J. C., 1965. Attenuation of elastic waves in granular medium, *J. geophys. Res.*, **70**, 3935–3942.

Scholz, C. H., 1968. Microfractures, aftershocks, and seismicity, *Bull. seism. Soc. Am.*, **58**, 1117–1130.

Scholz, C. H., Molnar, P. & Johnson, T., 1972. Detailed studies of frictional sliding of granite and implications for the earthquake mechanism, *J. geophys. Res.*, **77**, 6392–6406.

Utsu, T., 1961. A statistical study on the occurrence of aftershocks, *Geophys. Mag.*, **30**, 521–605.

Utsu, T., 1969. Aftershocks and earthquake statistics (I), *J. Fac. Sci. Hokkaido Univ.*, Ser. VII, **3**, 129–195.

Utsu, T., 1970. Aftershocks and earthquake statistics (II), *J. Fac. Sci. Hokkaido Univ.*, Ser. VII, **3**, 197–266.

Utsu, T., 1971. Aftershocks and earthquake statistics (III), *J. Fac. Sci. Hokkaido Univ.*, Ser. VII, **3**, 379–441.

Utsu, T., 1974. Space-time pattern of large earthquakes occurring off the Pacific coast of the Japanese islands, *J. Phys. Earth*, **22**, 325–342.

Utsu, T. & Seki, A., 1955. Relation between the area of aftershock region and the energy of main shock (in Japanese), *ZISIN*, Ser. II, **7**, 233–240.

Downloaded from http://gji.oxfordjournals.org/ at Library of Research Reactor Institute, Kyoto University on December 7, 2014